Dynamics of the Low-Level Jet off the West Coast of Subtropical South America

RICARDO C. MUÑOZ AND RENÉ D. GARREAUD

Department of Geophysics, University of Chile, Santiago, Chile

ABSTRACT

The subtropical west coast of South America is under the influence of the southeast Pacific anticyclone year-round, which induces persistent southerly winds along the coast of north-central Chile. These winds often take the form of a low-level coastal jet, in many aspects similar to the coastal jet existing off the California coast. Extensive diagnostics of mesoscale model results for a case in October 2000 are used here to describe the mean momentum budget supporting the coastal jet. The jet appears to occur when mid-latitude synoptic conditions induce a northerly directed pressure gradient force along the coast of north-central Chile. The very steep coastal terrain precludes the development of a significant easterly low-level wind that would geostrophically balance the pressure gradient. Instead, the meridional flow accelerates until turbulent friction in the marine boundary layer balances the meridional pressure gradient. The resulting force balance is semigeostrophic, with geostrophy valid only in the zonal (cross shore) direction. At higher levels, the topographic inhibition of the easterlies relaxes, and a small easterly flow ensues, which turns out to be very important in the temperature and stability budgets of the layer capping the marine boundary layer.

1. Introduction

The low-level wind regime in the southeast Pacific is dominated by a quasi-permanent subtropical high pressure system. Off the western coast of South America, along the coast of north and central Chile (latitude 37°–20°S), this high pressure system induces southerly winds, which in many instances take the form of a low-level coastal jet (CJ). In a companion paper (Garreaud and Muñoz 2005, hereafter GM05) we have used observed data and model results to document the existence of this CJ, characterize its climatology, and describe its structure. In this paper, we use mainly model results to investigate the main terms in the force budget associated with the CJ. We also discuss the turbulence and temperature budgets, as they relate to the dynamical balance. Our purpose is to improve the understanding of the underlying physical mechanisms controlling the intensity of the CJ, and its horizontal and vertical position. In the next section, we present a brief literature review of a CJ off the western coast of North America, which has similarities to the one discussed here. Section 3 summarizes the relevant results of GM05 including a description of the case study, verification of the model results, and characterization of the mean structure of the CJ. Section 4 describes the dynamical balance of the CJ and its related factors. In section 5 we discuss the results, and in section 6 we present our conclusions.

Corresponding author address: Dr. Ricardo C. Muñoz, Departamento de Geofísica, Universidad de Chile, Blanco Encalada 2002, Santiago, Chile.
E-mail: rmunoz@dgf.uchile.cl

2. Literature review

In this section, we present a brief review of literature concerning the CJ that exists off western North America, along the coast of California. It is not a comprehensive survey of the topic, but rather we have selected papers that through observations and/or modeling have addressed the structure and forcings of this CJ. As will become evident from our results, the CJ along the western coast of South America is in many aspects a close relative of the California CJ.

Bridger et al. (1993) show observations of the structure of the marine boundary layer (MBL) approximately 200 km off the coast of central California, taken during the Marine Atmospheric Boundary Layer Experiments, West Coast (MABLES-WC) experiment (Lester 1985). They distinguish a typical summertime condition in which there is a well-defined inversion, an inland trough in the surface pressure field, and no

large-scale synoptic disturbances. In their results, however, the best example of the CJ occurs during so-called "atypical" synoptic conditions, in which the pressure gradient near the coast is weaker, and only a coastal trough is observed (see their Fig. 5b). In this case the jet is located in the temperature inversion capping the MBL, and reaches speeds of up to 17 m s^{-1} at levels ~300 m ASL. Although there is no attempt to characterize the momentum budget of the jet, it is noted that in the atypical case the horizontal temperature gradient is larger than in the typical cases, and the observed vertical shear is parallel to the thermal wind vector.

Parish (2000) analyzes observations of the MBL structure off central California for two episodes in which wind speed maxima extending more than 100 km from the coast are observed. In both cases maximum wind speeds over 25 m s^{-1} are measured in the inversion capping the MBL. By measuring the slope of orthogonal isobaric heights, he finds that the jet is in a state of near-geostrophic balance, and that thermal wind balance is sustained by the slope of the MBL and isotherms above. He explains the CJ as the geostrophic adjustment of a thermally direct circulation forced by the thermal contrast between land and ocean. Pomeroy and Parish (2001) expand the analysis to a third case from the same experiment, confirming the observations of Parish (2000) and observing that the scale of the CJ suggests that it is not closely related to local coastal terrain features.

Chao (1985) presents a theoretical investigation about the forcing of the CJ along the west coast of North America, using a shallow water analytical model. He mainly addresses the horizontal distribution of wind speed and discusses separately the topographic and thermal effects on the CJ. His results show that the coastal mountain barrier's inhibition of zonal winds can generate an equatorward jet with a horizontal structure similar to the observed, that is, with maximum speeds around 30°N and a width scale ~1000 km. The CJ in the model is forced by large-scale zonal winds that generate Kelvin waves along the coast, captured by friction at a state of equilibrium. The pure topographic effect, though, underestimates the strength of the jet and cannot explain its summertime intensification. The pure thermal effect, on the other hand, produces a more symmetric jet across the coastal line. Chao's conclusion is that the main forcing of the observed jet is the topographic barrier effect, modulated by other factors like the thermal and roughness contrast between land and ocean, as well as nonlinear effects.

Cui et al. (1998) show results of idealized mesoscale simulations of the coastal flow along central California. They obtain results for eight cases, each having a different direction in the large-scale pressure gradient. All cases develop a low-level jet parallel to the coast, although the flow can be from the NW or from the SE. The main controlling factor is the onshore or offshore component of the imposed background geostrophic flow. In cases with an offshore component, a northwesterly CJ develops at the top of the MBL, which slopes markedly downward toward the coast. The shallower MBL at the coast and the large baroclinity above is said to be controlled by the cross-coast flow and its interaction with the topography. The CJ maintains a semigeostrophic balance, in which along the coast the background pressure gradient plus the induced mesoscale pressure perturbation are balanced by turbulent and acceleration terms. Onshore flow due to a sea breeze or due to local across-coast pressure gradient perturbations is held responsible for accelerating the along-coast flow through Coriolis deflection.

Bielli et al. (2002) apply a numerical mesoscale model to simulate the summertime low-level flow along the central Oregon coast. They describe a 4-day period in which the mean surface wind speed field at 200 m above sea level (ASL) shows a broad maximum of ~18 m s^{-1} at about 200 km off the coast of southern Oregon and northern California. Their focus is on the MBL to the north of the jet, finding that in this region advection is an important term in the meridional momentum budget, along with the alongshore pressure gradient. The latter is hypothesized to be due to heating over the mountains in southern Oregon and northern California. The cross-shore momentum balance, on the other hand, is found to be geostrophic.

Burk and Thompson (1996) model a summertime CJ along the California coast. In their control run the jet speeds up to 22 m s^{-1} at the MBL top, about 50 km from the coast. They show that the jet is associated with strong baroclinity at the coast, manifested in the eastward-sloping MBL, and caused by the differential heating of the sea and the continent. They discard effects of sea surface temperature gradients in controlling the MBL slope and consider that it is more the result of dynamically enhanced (suppressed) subsidence at the left entrance (right exit) side of the CJ. In their results coastal topography modulates the CJ features by generating a warm layer capping the MBL, especially downstream of coastal points and capes.

In summary, the California CJ is a maximum in N-NW winds that occur near the top of the MBL, with a cross-shore scale of ~500–1000 km. The cross-shore pressure gradient is associated with a MBL sloping downward toward the coast, maintaining a near-geostrophic equilibrium with the Coriolis deflection of the jet. In contrast, in the along-coast momentum bal-

ance turbulence and advection play an important role. The cross-shore flow appears to be very relevant in the CJ balance, though different mechanisms are postulated: Coriolis deflection of a sea-breeze-type circulation, induced warming of the layer above the MBL, induced subsidence/upsidence at the flanks of the CJ, and subgeostrophy due to the topographic restriction.

3. Case study and model verification

As described in GM05, we have used the Pennsylvania State University–National Center for Atmospheric Research (PSU–NCAR) Mesoscale Model (MM5; Grell et al. 1994) to simulate the Crucero de Investigación Marina (CIMAR-6) period from 0600 UTC 1 October 2000 until 1800 UTC 21 October 2000 (official time in Chile is UTC−4). During this 20-day period the coastal jet was present at 30°S between 4 and 15 October. Particularly steady conditions in the position and intensity of the jet were found in the period 0000 UTC 9 October–0000 UTC 11 October. The averages discussed hereafter are averages over these 3 days, unless otherwise noted.

Figure 1a shows domain 2 of the model runs (horizontal resolution 45 km) and contours of the model topography. Figure 1b shows the very homogeneous stratocumulus (Sc) cover existing at 1414 UTC 11 October 2000, together with the Quick Scatterometer (QuikSCAT) wind field at 1107 UTC of the same day (every other wind vector is plotted). The CJ is observed in the maximum wind speeds found near the coast at ~30°S. Figures 1c and 1d show the near-surface pressure field and the 500-hPa geopotential height computed by the model at 1200 UTC 11 October 2000. The subtropical anticyclone is centered around 31°S but extends to the ESE producing maximum coastal surface pressures around 35°S. To the south the surface pressures decrease uniformly, while to the north there is a coastal trough. The upper-level pressure field shows a rather uniform descent of the geopotential heights from north to south over the full domain. The WSW flow aloft is indicative of a weak ridge approaching the region from the west.

The conclusions of GM05 are partly summarized in Figs. 2–4. Figures 2a and 2b show the mean surface wind speeds over the ocean obtained from the QuikSCAT data and the model results, respectively. The model reproduces very well the horizontal structure of the wind field, especially the maximum close to the coast at 30°S. Part of the structure in these mean fields, particularly south of 35°S, is due to the shapes of the QuikSCAT swaths, which do not cover the full region, nor do they have the same shape always. Since the average shown considers only six QuikSCAT swaths, the mean field results with some unphysical structure. The modeled field retains a similar structure, because it was taken for exactly the same points and times for which there were QuikSCAT data available. Figure 2c shows time series of surface wind speed for a point located in the region of maximum wind speeds (marked with a cross in Figs. 2a and 2b). The closed circles in Fig. 2c are the twice-daily QuikSCAT wind speed, and the line with open circles is the model output for the same point. The model reproduces well the time variability of the wind speed at this location, which is characterized by a period of larger wind speeds between 4 and 15 October 2000. In the data and the model, the amplitude of the diurnal cycle in wind speed off the coast is small compared to the synoptic variability.

Figure 3 shows mean meridional cross sections taken along a line passing through the jet axis. Figures 3a–d show zonal wind, meridional wind, vertical velocity, and temperature, respectively. Shading in this and subsequent figures denote regions with meridional wind (V) greater than 19 m s^{-1}. The CJ in this period is centered at about 30°S, at ~350 m ASL, immersed in the temperature inversion capping the MBL. Above the jet, the mean zonal wind is weak and offshore, while in the MBL it is onshore. Subsidence prevails upwind of the jet, but a positive mean vertical velocity is found downstream of the jet maximum. The maximum meridional temperature gradient is observed in the region above the MBL, to the south of the jet. The maximum vertical temperature gradient (stability), on the other hand, coincides roughly with the jet core. Figure 4 shows mean zonal cross sections of V and temperature, taken at 30°S, close to the position of the jet center. The sloping of the MBL downward toward the coast is evident in these figures, from about 1000 m at 79°W, to ~300 m at 73°W near the coast. Figure 4b shows that there exists a large zonal temperature gradient in the coastal region above the MBL.

The figures above illustrate the similarities between the CJ discussed here and the one off the coast of California described in section 2. This CJ also resides in the inversion layer capping the MBL, which slopes markedly downward to the coast. Its cross-coast scale is about 500–1000 km. Other characteristics of this CJ's climatology described in GM05 are its relatively small diurnal cycle, large synoptic variability, and a seasonal cycle characterized more by a change in latitude and frequency than a change in intensity. In the next section, we expand the diagnostics of the model results, describing the main terms of the momentum balance supporting the CJ.

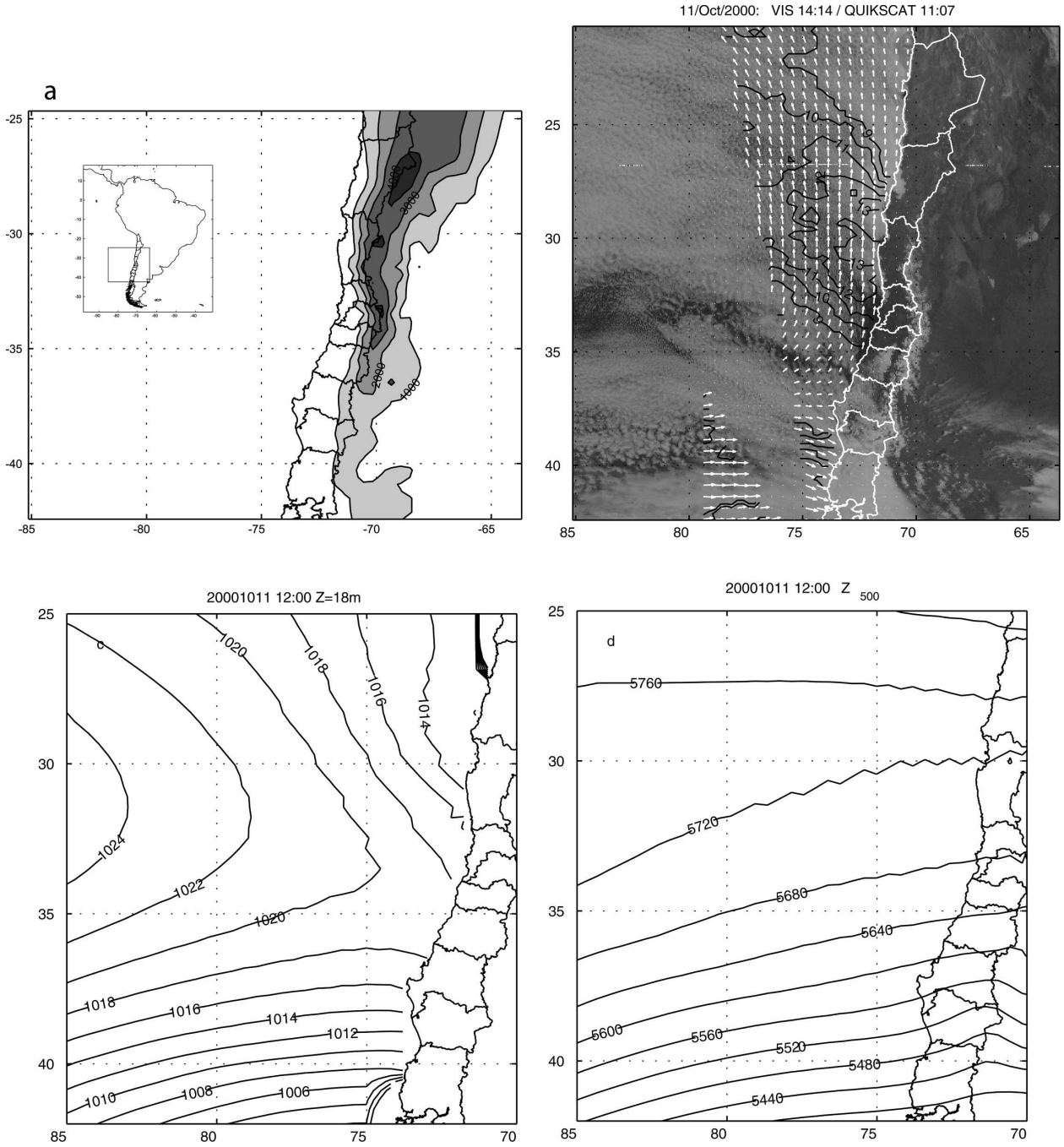

FIG. 1. (a) Domain 2 of MM5 model runs. Shaded contours mark model topography at 1000, 2000, 3000, and 4000 m ASL. Inset shows a map of South America with box over model domain. (b) Visible Geostationary Operational Environmental Satellite (GOES) image at 1414 UTC 11 Oct 2000, and QuikSCAT wind vectors and contours of wind speed (m s^{-1}) for 1107 UTC 11 Oct 2000. (c) Model-computed pressure (hPa) at 18 m ASL for 1200 UTC 11 Oct 2000. (d) Model-computed 500-hPa geopotential height (m) for 1200 UTC 11 Oct 2000. Coastline and regional administrative divisions of Chile are marked in (a)–(d) by fine lines.

4. Balances of the jet

a. Computation of budgets

Outputs of the model every 2 h were used to compute the momentum and temperature budgets averaged over the 3-day period mentioned above. All variables were first interpolated to a constant-z grid, and then the spatial gradients needed in the computation of the advective and pressure gradient terms in the budgets were calculated using a centered finite-difference scheme.

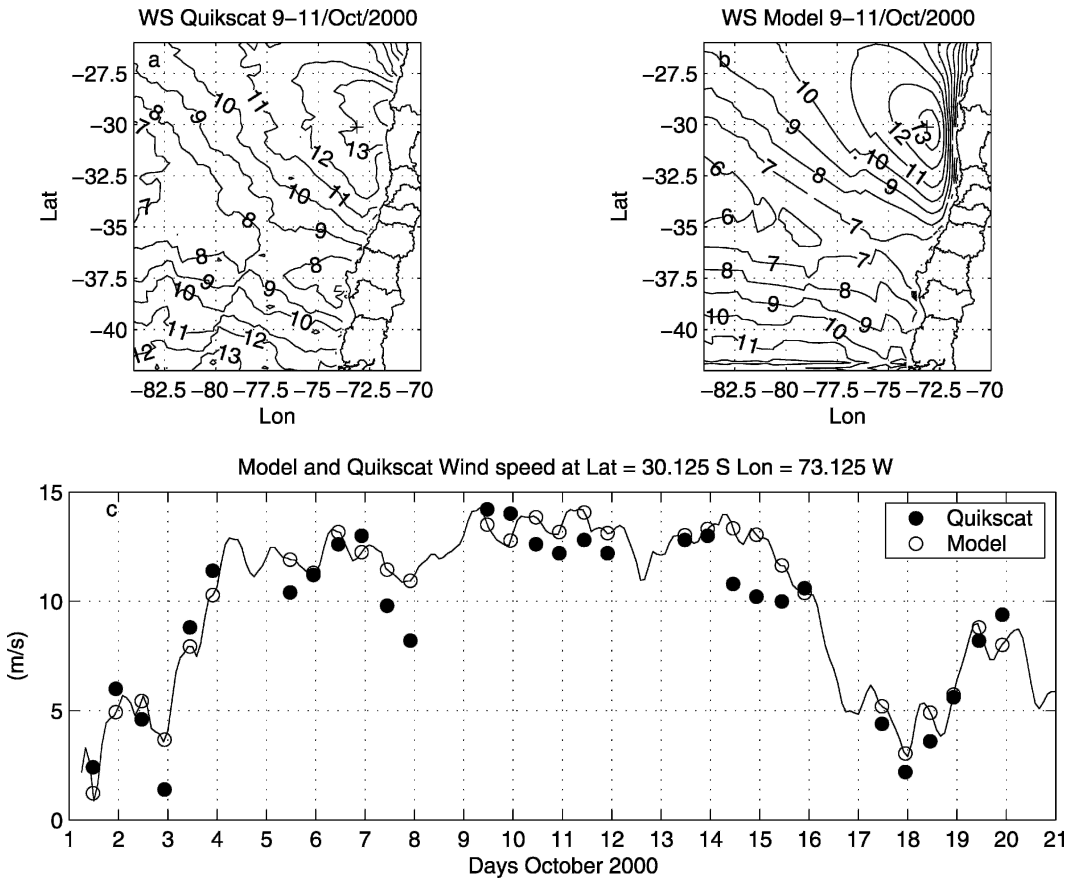

FIG. 2. Comparison of model results and QuikSCAT data. (a) QuikSCAT mean surface wind speed for the period 9–11 Oct 2000. (b) Model mean surface wind speed for the period 9–11 Oct 2000. (c) Time series of QuikSCAT (filled circles) and model (line and open circles) wind speed for a point located at 30.125°S lat, 73.125°W lon [location marked with a cross in (a) and (b)]. Speed in m s^{-1}.

The vertical diffusion was computed with the same 1.5-order turbulence scheme used in the mesoscale model runs (Gayno 1994; Shafran et al. 2000), and the same was done with the horizontal diffusion. The thermodynamic energy budget was computed using the liquid water potential temperature, Θ_l, defined as

$$\Theta_l = \Theta - \frac{\Theta}{T}\frac{L}{c_p} q_c, \tag{1}$$

where T and Θ are temperature and potential temperature, respectively, q_c is the liquid water content, L is the latent heat of evaporation, and c_p is the specific heat at constant pressure. The advantage of using Θ_l as the thermodynamic variable is that it is approximately conserved for condensation/evaporation processes, and it reduces to Θ when there is no liquid water present in the grid point (Deardorff 1976). The Θ_l budget is computed combining the budgets of Θ (based upon the budget of T) and q_c following (1).

b. *Momentum budget*

We consider first the meridional momentum budget, which can be written as

$$\frac{\partial V}{\partial t} = -U\frac{\partial V}{\partial x} - V\frac{\partial V}{\partial y} - W\frac{\partial V}{\partial z} - \frac{1}{\rho}\frac{\partial P}{\partial y} - fU + V_m, \tag{2}$$

where, from left to right, the terms correspond to local time change, zonal, meridional, and vertical advection, pressure gradient, Coriolis, and mixing (symbolically written as V_m, and including vertical and horizontal diffusion). In (2) U, V, and W are the components of the wind vector, ρ is air density, and f is the Coriolis parameter. Figure 5 shows the mean horizontal distribution of the main terms in this budget for the model level at 312 m ASL (the level of maximum V near the coast). Figure 5a shows the pressure gradient (PG) accelera-

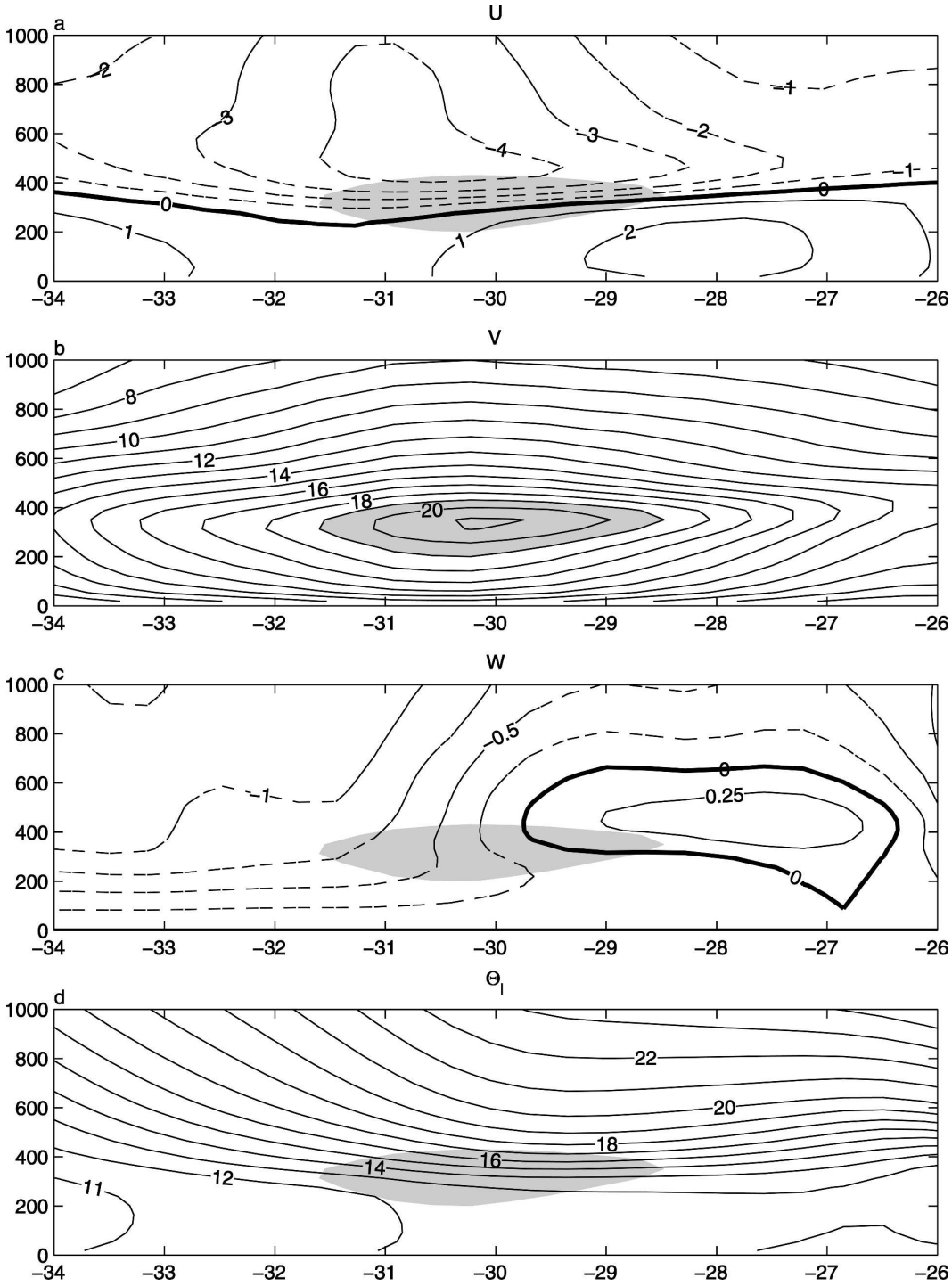

FIG. 3. Mean meridional cross sections at 72.8°W. (a) Zonal wind (m s^{-1}), (b) meridional wind (m s^{-1}), (c) vertical velocity (cm s^{-1}), and (d) liquid water potential temperature (°C). Shading marks region with $V > 19$ m s^{-1}. In all panels, vertical axis is height ASL (m) and horizontal axis is latitude (°).

tion. South from 34°–35°S this term is negative and shows little longitudinal variation. To the north, however, this term is positive and possesses a rich structure. West of ~78°W the field tends to be very zonal, while to the east and closer to the coast the PG acceleration intensifies greatly with a peak of ~3.5 m s^{-1} h^{-1} right at the coast at 31°S. The PG term decreases rapidly to the north, reaching ~ −0.5 m s^{-1}

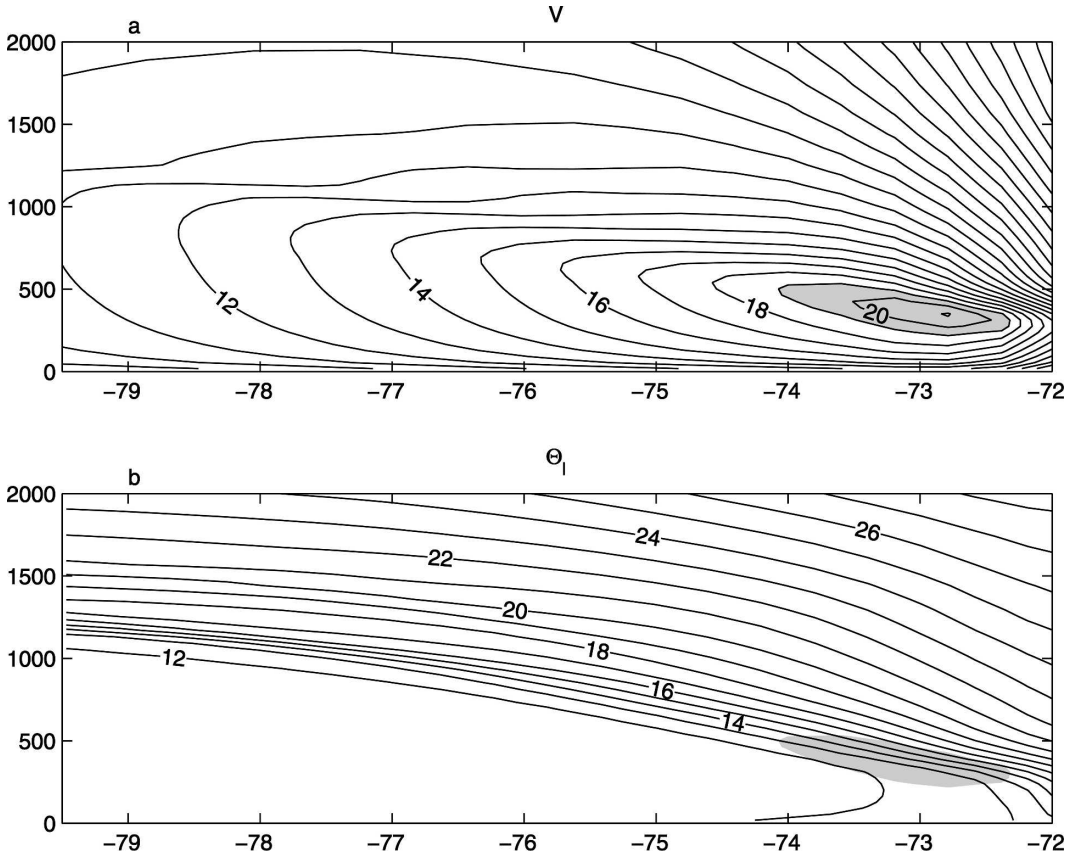

FIG. 4. Mean zonal cross sections at 30°S. (a) Meridional wind (m s^{-1}) and (b) liquid water potential temperature (°C). Shading marks region with $V > 19$ m s^{-1}. In both (a) and (b) vertical axis is height ASL (m) and horizontal axis is longitude (°).

h^{-1} at 27°S. Thus, north of 35°S there appears to be a coastal disturbance in the pressure field that extends about 500 km into the sea and spans about 1000 km along the coast. Figures 5b–d show the Coriolis, horizontal (zonal plus meridional) advection, and mixing terms of the V budget, respectively. Comparison of the four panels shows that the pressure gradient and the Coriolis terms are the main components of the budget everywhere, except in the region of the coastal pressure disturbance. In this region the PG term is very strong, while the magnitude of the Coriolis acceleration is near zero. Consequently, the PG term is balanced there by the horizontal advection and the mixing terms, both of which have their maximum magnitudes in this coastal region. The advective term (Fig. 5c) is negative to the south of the jet, and positive to the north. The shape of the mixing term field (Fig. 5d), on the other hand, resembles that of the meridional velocity (see Fig. 6b) with a peak almost collocated with the jet.

Analogous to (2), the zonal momentum equation can be written as

$$\frac{\partial U}{\partial t} = -U\frac{\partial U}{\partial x} - V\frac{\partial U}{\partial y} - W\frac{\partial U}{\partial z} - \frac{1}{\rho}\frac{\partial P}{\partial x} + fV + U_m. \tag{3}$$

The horizontal distribution of the terms in the zonal momentum budget is shown in Fig. 6. The pressure gradient and Coriolis terms (Figs. 6a,b) are the main components in the balance everywhere, showing that over open ocean *and* near the coast the zonal momentum budget is close to geostrophy, that is,

$$0 \approx -\frac{1}{\rho}\frac{\partial P}{\partial x} + fV. \tag{4}$$

Thus, the meridional velocity is near its geostrophic value, $V \approx V_g \equiv (1/\rho f)\,(\partial P/\partial x)$. On the other hand, the zonal velocity U is very subgeostrophic, as shown in Fig. 7, where contours of the ageostrophic components (U–U_g) and (V–V_g) at 312 m ASL are drawn. Figure 7a shows that the zonal ageostrophic wind reaches maximum values in the coastal region south of ~30°S, which accounts for the large meridional acceleration giving

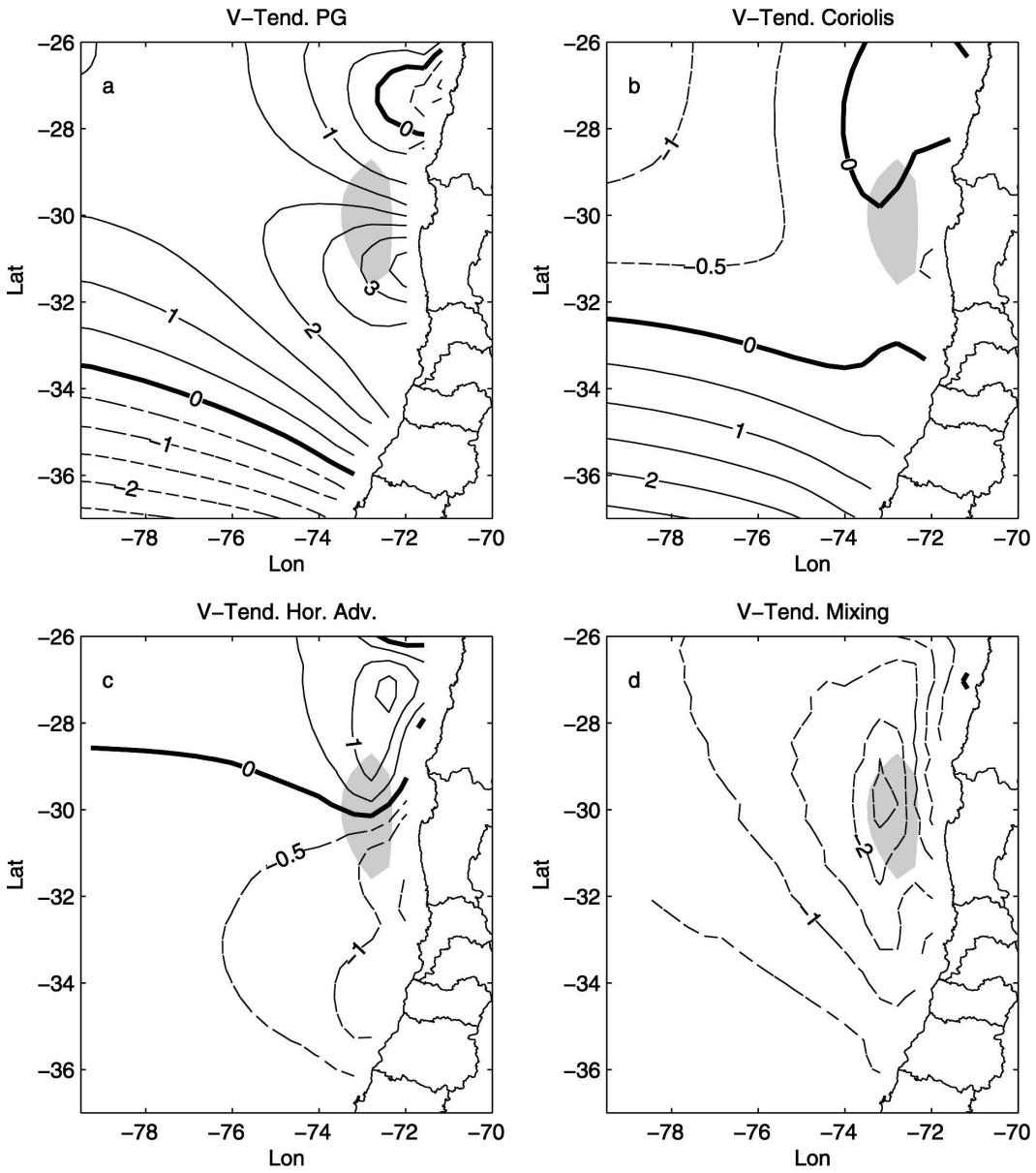

FIG. 5. Model-derived terms of the meridional momentum budget at 312 m ASL averaged for the period 9–11 Oct 2000. (a) Pressure gradient, (b) Coriolis, (c) horizontal advection, and (d) mixing. Contour values in m s^{-1} h^{-1}. Only grid points over the ocean have been contoured. Shading marks region with $V > 19$ m s^{-1}.

rise to the jet. The meridional ageostrophic wind (Fig. 7b), on the other hand, has much smaller values. In the free troposphere, say at ~4000 m ASL, the ageostrophic zonal flow is considerably smaller, with little structure and values between -1 and -2 m s^{-1} (not shown).

The vertical profiles of the terms in the zonal and meridional momentum budgets are shown in Figs. 8a and 8b, respectively, for a grid point closest to the location of the jet center. Let us consider first the profiles above ~2000 m, that is, well above the MBL. In the meridional momentum budget (Fig. 8b), the PG term is negative, implying that pressures increase to the north, as observed also in Fig. 1c. The magnitude of the PG term increases in this region linearly with height and it is balanced mainly by the Coriolis acceleration, reflecting a near-geostrophic condition. The zonal PG term (Fig. 8a) above ~2000 m is relatively small and also balanced mainly by the Coriolis term. In the lower layers, the mean momentum budgets change dramatically. The meridional pressure gradient reverts sign at ~2000 m and its magnitude increases downward until the sur-

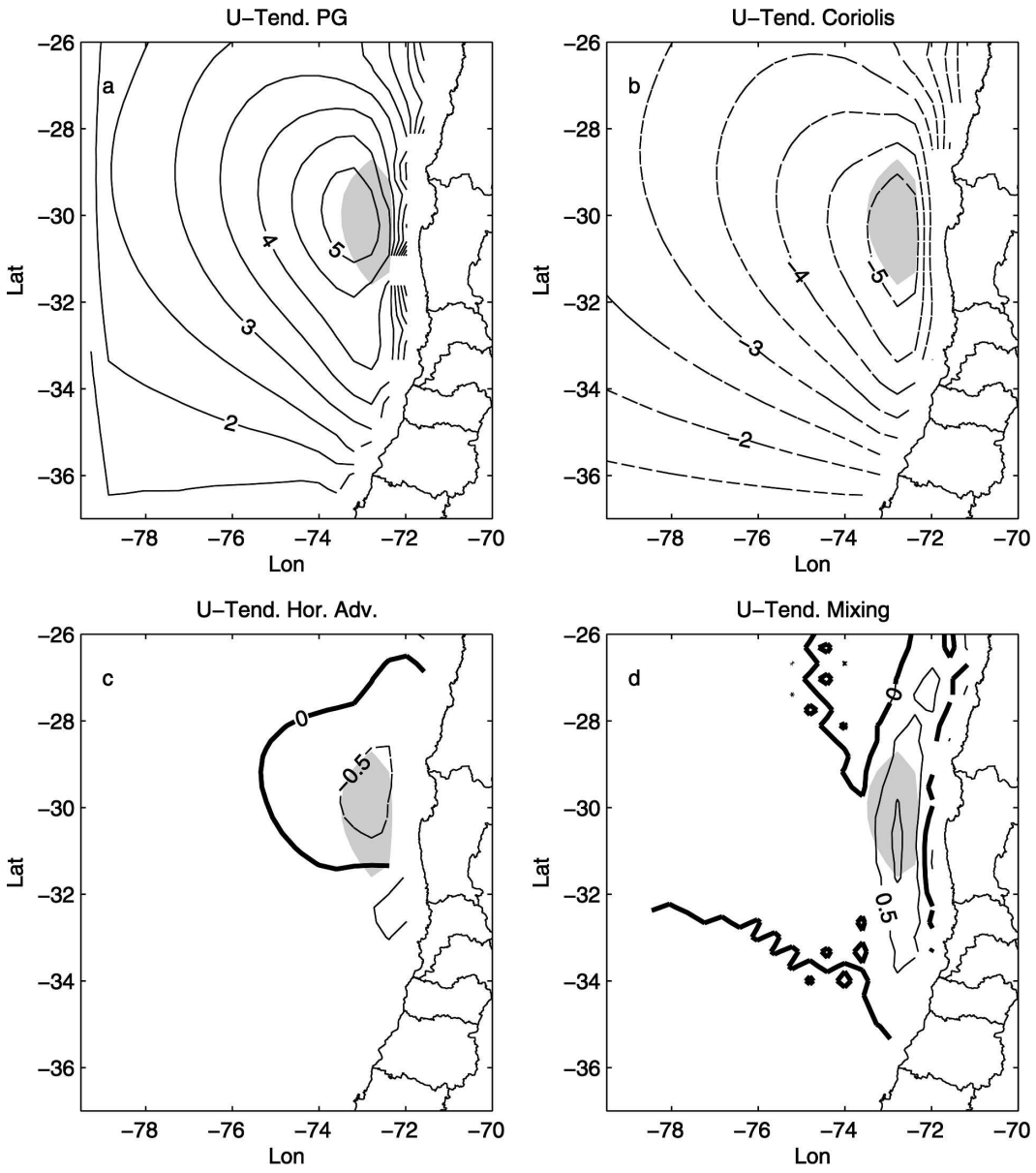

FIG. 6. Model-derived terms of the zonal momentum budget at 312 m ASL averaged for the period 9–11 Oct 2000. (a) Pressure gradient, (b) Coriolis, (c) horizontal advection, and (d) mixing. Contour values in m s^{-1} h^{-1}. Only grid points over the ocean have been contoured. Shading marks region with $V > 19$ m s^{-1}.

face. In this region, the Coriolis term is insufficient to balance the PG, resulting in a nongeostrophic condition in which advection, friction, and Coriolis are important. Above the MBL Coriolis and advection balance the PG, while in the turbulent BL below ~400 m, friction is the dominant balance of the PG. The zonal momentum, on the other hand, remains close to geostrophy over the full column. Thus, it is apparent from these vertical profiles that suppression of significant easterly winds at low levels is a key factor to explain the acceleration of the meridional flow and the maintenance of the CJ.

We turn to the question of the latitudinal location of the jet center (30°S in this period). Figure 9a shows the mean profile of meridional speed (V) at 312 m ASL along a line passing through the jet axis (longitude ~72.8°W). The analysis of the momentum budget has shown that in the meridional direction, turbulent and advection play an important role in balancing the meridional pressure gradient acceleration. Figure 9b illustrates this balance by plotting the meridional profile of the sum of the PG and Coriolis terms together with ($-V_m$). Neglecting the remaining terms in (1) the dif-

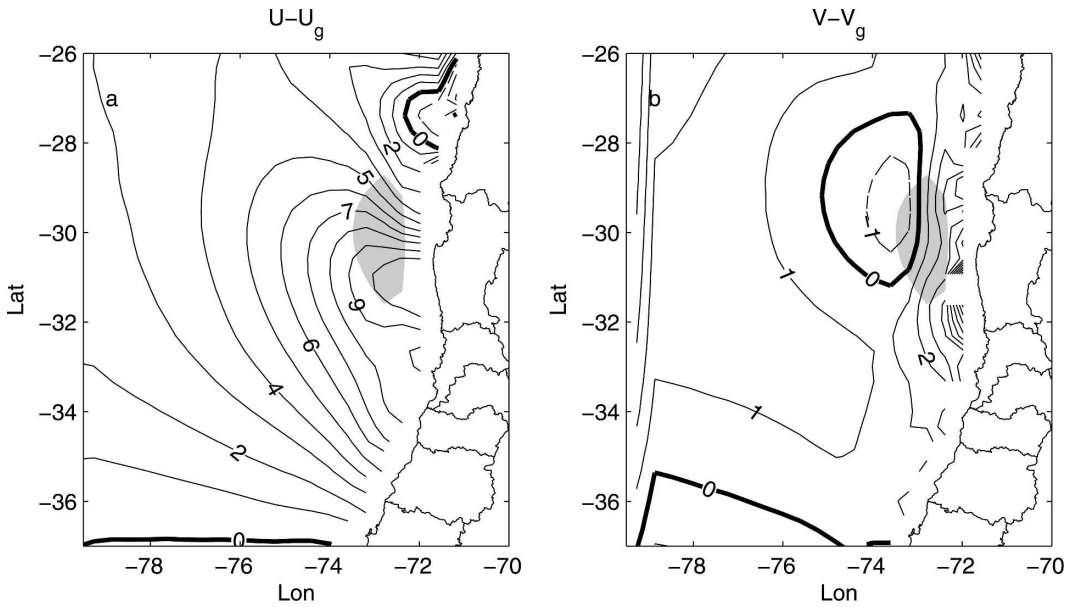

FIG. 7. Ageostrophic (a) zonal and (b) meridional winds at 312 m ASL averaged for the period 9–11 Oct 2000. Contours in m s^{-1}. Shading marks region with $V > 19$ m s^{-1}.

ference between both profiles in Fig. 9b represents the advective acceleration of the flow. South (north) of 30°S this difference is positive (negative), explaining the increase (decrease) of meridional speed in Fig. 9a. From this figure, it is apparent that the maximum meridional speed is located where turbulent friction and mixing balance the other terms in the budget. It is therefore of interest to understand the factors controlling the meridional variation of the turbulence, which is done next.

c. Turbulence and temperature budgets

The contours of the mean turbulent kinetic energy (TKE) shown in Fig. 10a illustrate the meridional structure of the MBL along the CJ axis. Maximum values of TKE are found in the bottom part of the MBL, and at the latitude of the CJ center. Figure 8d shows the main terms in the TKE budget at the jet location. There is a close equilibrium between shear production and dissipation, with buoyant production playing only a minor role. Thus, in these model results turbulence in the MBL is dominated by mechanical production associated with the shear induced by the CJ. Since the model produced less cloud cover at the top of the MBL as compared to the visible satellite images, the modeled TKE budget could be underestimating the importance of the buoyant production. Brost et al. (1982) have shown observations of the TKE budget in the Sc-capped MBL off California, in which the shear production at the bottom part of the MBL is also the main production term. Moreover, their numerical values of shear production are comparable with those obtained in the present case.

A striking feature in Fig. 10a is the modest variation of the depth of the turbulent layer along the jet axis. Burk and Thompson (1996) describe a similar result in their simulation of the California CJ. They argue that a channel flow analogy might suggest that the acceleration of the flow along the jet axis should be accompanied by a *shallowing* of the MBL. In their interpretation, the latter does not happen because it is offset by the enhanced entrainment at the MBL top due to the increased turbulence at the jet location. However, without recourse to the channel flow analogy, and only considering boundary layer dynamics, one might also ask why the MBL is not *deeper* at the jet location because of the enhanced turbulence below the jet core. The answer appears to be in the stability capping the MBL. Figure 10b shows the mean contours of the Brunt–Väisälä frequency along the same axis as Fig. 10a. The region of the jet is not only a maximum in meridional velocity but it is also a region of maximum stability. Our interpretation is that in spite of the MBL being more turbulent below the jet core, it is not deeper because the stability capping it is also much larger. While turbulence in the modeled MBL is dominated by shear production, the vertical extent that this mechanically produced turbulent layer can reach is controlled in part by the stability of the layer above.

Finally, we address the factors producing the region

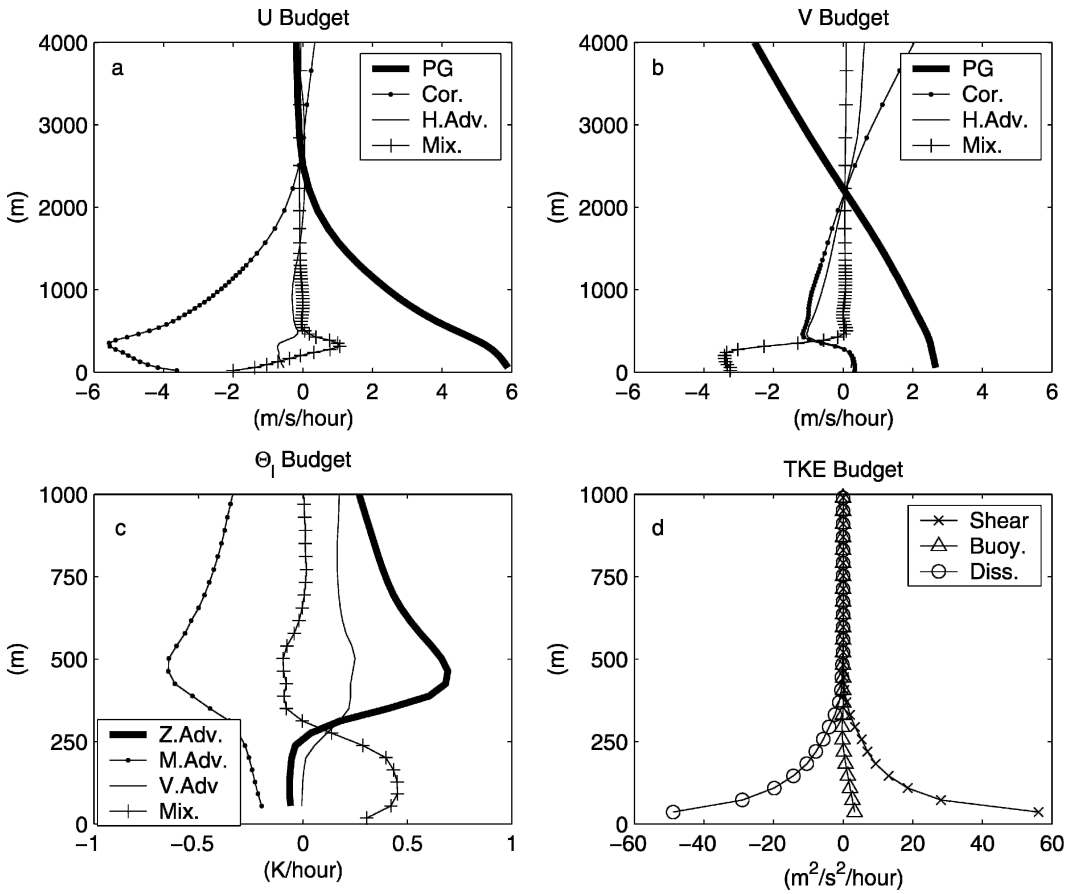

FIG. 8. Mean vertical profiles of terms in the budgets of (a) zonal momentum, (b) meridional momentum, (c) liquid water potential temperature, and (d) turbulent kinetic energy, for point at 30.2°S, 72.8°W.

of maximum stability at the jet's core. For this purpose, we consider the Θ_l budget, written as

$$\frac{\partial \Theta_l}{\partial t} = -U\frac{\partial \Theta_l}{\partial x} - V\frac{\partial \Theta_l}{\partial y} - W\frac{\partial \Theta_l}{\partial z} + \Theta_{l,r} + \Theta_{l,m}. \tag{5}$$

The last two terms in (5) denote the radiative tendency and the mixing (vertical and horizontal) terms, respectively. The vertical profiles of the different terms in the modeled Θ_l budget are shown in Fig. 8c for a point at the jet core. Above the MBL, the advective terms are the dominant terms in this budget. In particular, zonal advection has a vertical structure that tends to maximize the stability capping the MBL.

The meridional structure of the advective terms in the Θ_l budget is shown in Fig. 11. Figures 11a–c show meridional cross sections of the zonal, meridional, and vertical advections, respectively. In spite of being small compared to its geostrophic value, Fig. 11a shows that the easterly zonal wind is very important in the Θ_l budget. It produces maximum heating rates right at and above the location of the jet core (i.e., at ~30°S in this case) by advection of warmer air from the continent. The meridional and vertical advections of temperature have similar but opposite structure. To the south of the jet, enhanced subsidence produces a positive temperature tendency, while the opposite is true to the north of the jet. Meridional advection, on the other hand, produces negative temperature tendencies to the south of the jet, and positive tendencies to the north. The net effect of the advective temperature tendencies is shown in Fig. 11d. There is net heating in the layer capping the MBL and cooling below. These tendencies are offset by the nonadvective Θ_l tendencies shown in Fig. 12. Turbulent diffusion in the vertical (Fig. 12a) warms the MBL, radiation (Fig. 12b) cools, especially the layer above the MBL, and horizontal diffusion has a mixed effect (though not negligible due to the large horizontal temperature gradients near the coast). The net effect of the nonadvective Θ_l tendencies is shown in Fig. 12d, which is similar but opposite in sign to the net advective tendencies of Fig. 11d. Although Figs. 11b and 11c show that meridional and vertical advective tendencies have

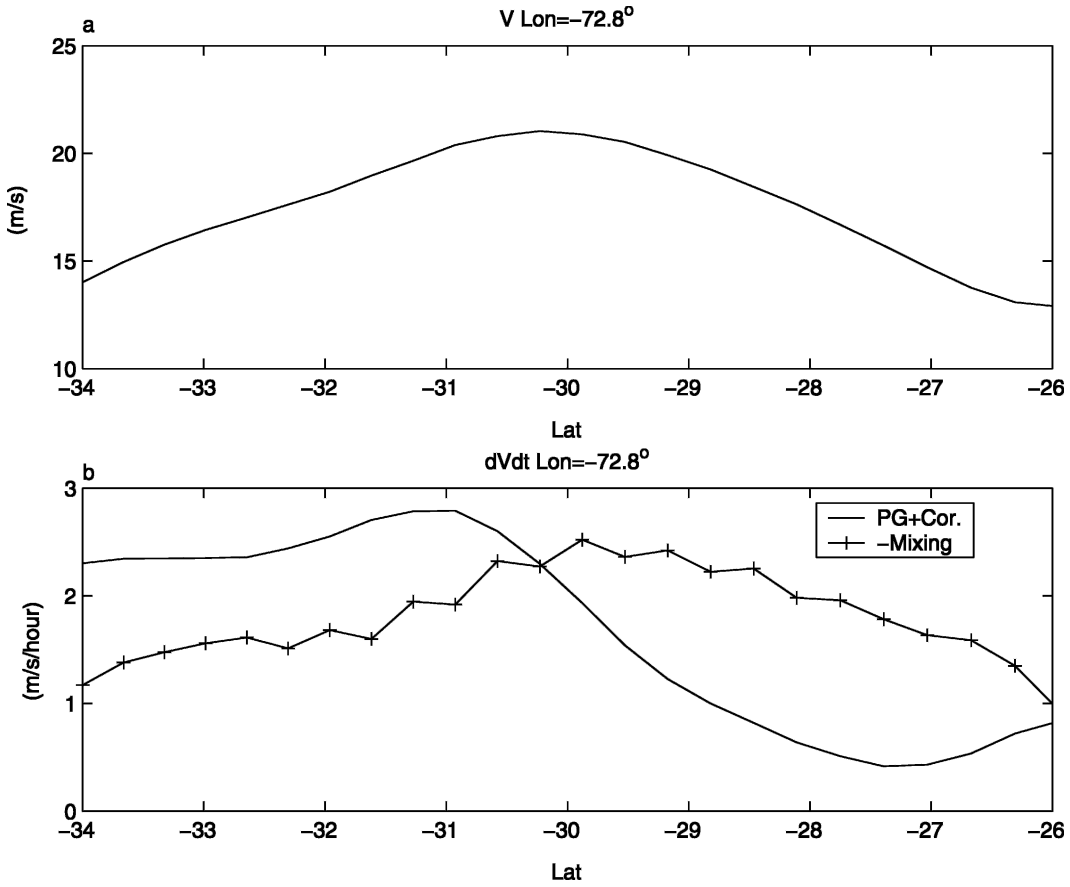

FIG. 9. Meridional profiles at 72.8°W and 312 m ASL averaged for 9–11 Oct 2000. (a) Meridional wind speed ($\mathrm{m\,s^{-1}}$), and (b) pressure gradient plus Coriolis accelerations (solid fine), with deceleration due to vertical and horizontal diffusion (line with crosses).

a similar but opposite structure, a close look at them shows that the meridional advection pattern is shifted with respect to the vertical advection pattern. At the latitude of the maximum V (~30°S), this shift is responsible of the warming due to the zonal temperature advection being primarily balanced by the meridional advection of cooler air. This balance between zonal and meridional thermal advection *at the location of the jet core* is evident also in the vertical profiles of Fig. 8c. The main conclusion here is therefore that the zonal advection of temperature is crucial to enhance the stability of the layer capping the MBL at the location of the jet, and that in this region zonal and meridional temperature advections are in close balance.

5. Discussion

a. Simplified balances (and spatial structure)

Based on the modeled budgets of momentum and temperature presented above, we can simplify them at the location of the jet as follows:

$$0 = -\frac{1}{\rho}\frac{\partial P}{\partial x} + fV, \tag{6}$$

$$0 = -fU + V_m, \tag{7}$$

$$0 = -U\frac{\partial \Theta_l}{\partial x} - V\frac{\partial \Theta_l}{\partial y}. \tag{8}$$

Thus, we consider a semigeostrophic balance in which a geostrophic force balance is observed only in the zonal direction. In the meridional direction, we approximate the budget including only the meridional pressure gradient and mixing, while in the temperature budget we balance the horizontal advective tendencies.

Using in (7) a simple Rayleigh friction model to approximate $V_m \sim -cV$ (with c being a constant), the above equations can be solved for U, V, and the zonal pressure gradient, assuming that the meridional PG and the horizontal temperature gradients are externally imposed conditions. The solution is then

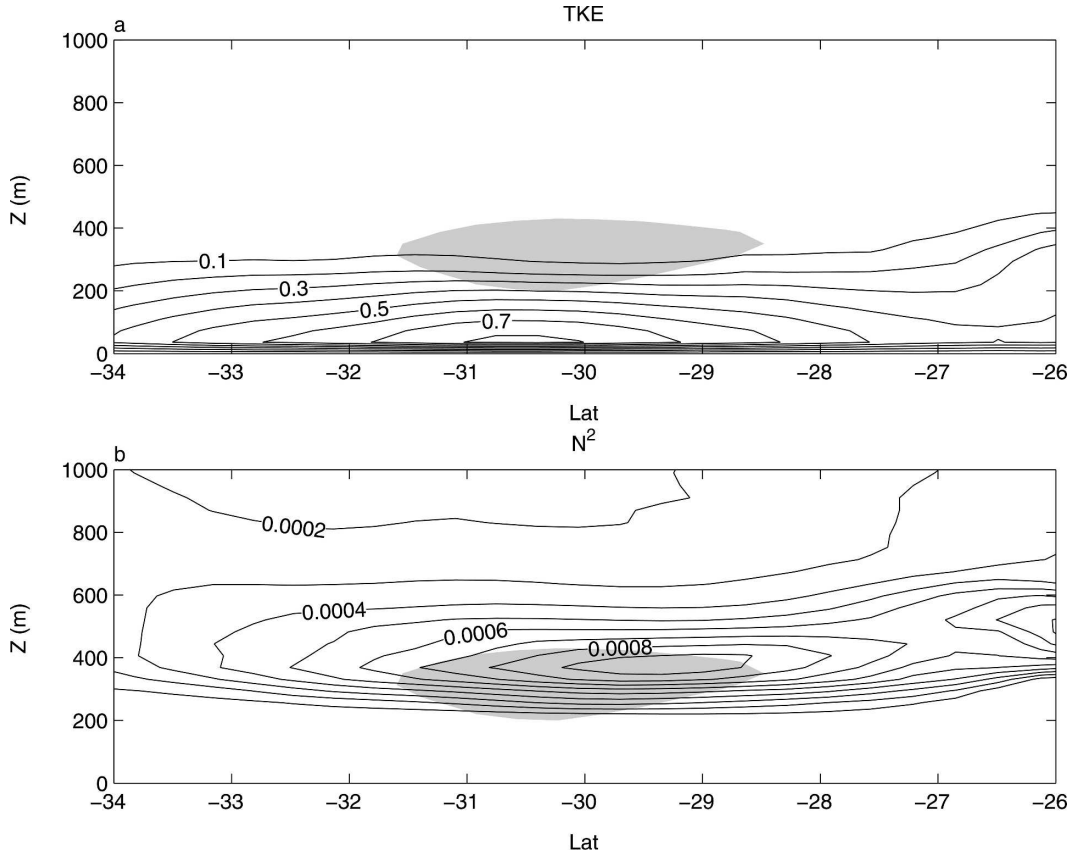

FIG. 10. Meridional cross sections at 72.8°W averaged for 9–11 Oct 2000. (a) Turbulent kinetic energy ($m^2\,s^{-2}$) and (b) Brunt–Väisälä frequency squared (s^{-2}). Shading marks region with $V > 19\ m\,s^{-1}$.

$$U = \frac{1}{c\rho}\left(\frac{\partial\Theta_l/\partial y}{\partial\Theta_l/\partial x}\right)\frac{\partial P}{\partial y}, \tag{9}$$

$$V = \frac{-1}{c\rho}\frac{\partial P}{\partial y}, \tag{10}$$

$$\frac{\partial P}{\partial x} = \frac{-f}{c}\frac{\partial P}{\partial y}. \tag{11}$$

Before analyzing these results, we note that $f < 0$ (Southern Hemisphere), $\partial P/\partial y < 0$ (the synoptic condition produces a high pressure to the south of the jet), $\partial\Theta_l/\partial x > 0$ (ocean–land thermal contrast), and $\partial\Theta_l/\partial y > 0$ (climatological equatorward thermal gradient). With these conditions, the flow responses are $V > 0$ (southerly flow), $U < 0$ (easterly zonal flow), and $\partial P/\partial x < 0$ (coastal trough).

The result in (11) can be visualized as a condition on the angle of the isobars approaching the coast. If we call this angle α, then (11) is equivalent to $\tan(\alpha) = |\partial P/\partial y|/|\partial P/\partial x| \sim c/|f|$. The coefficient c can be estimated from the model results by looking at Fig. 5d, which suggests $c \sim 5 \times 10^{-5}\ s^{-1}$. For a point at 30° S, we obtain $\alpha \sim 35°$. Therefore the isobars near the coast should produce a coastal trough with isobars making an angle of ~35° with the coastline. The formation of coastal troughs along the coast of central Chile is indeed a very ubiquitous feature of the sea level pressure field (Garreaud et al. 2002).

b. *Role of meridional pressure gradient (and synoptic variability)*

The result in (10) suggests that the magnitude of the jet should be closely related to the meridional pressure gradient. To determine if these results hold for synoptic-scale variations, we have calculated the local correlation coefficient (i.e., collocated grid boxes) between daily values of QuikSCAT meridional surface wind and the reanalysis meridional gradient of the 900-hPa geopotential height. The r^2 field is presented in Fig. 13, which shows a maximum over an area of ~500 km off the coast of central Chile. Thus, synoptic variations of the southerly winds over the coastal jet region are largely explained (up to 80% of the variance) by variations in the low-level alongshore pressure gradient. Similar results hold when varying the geopotential

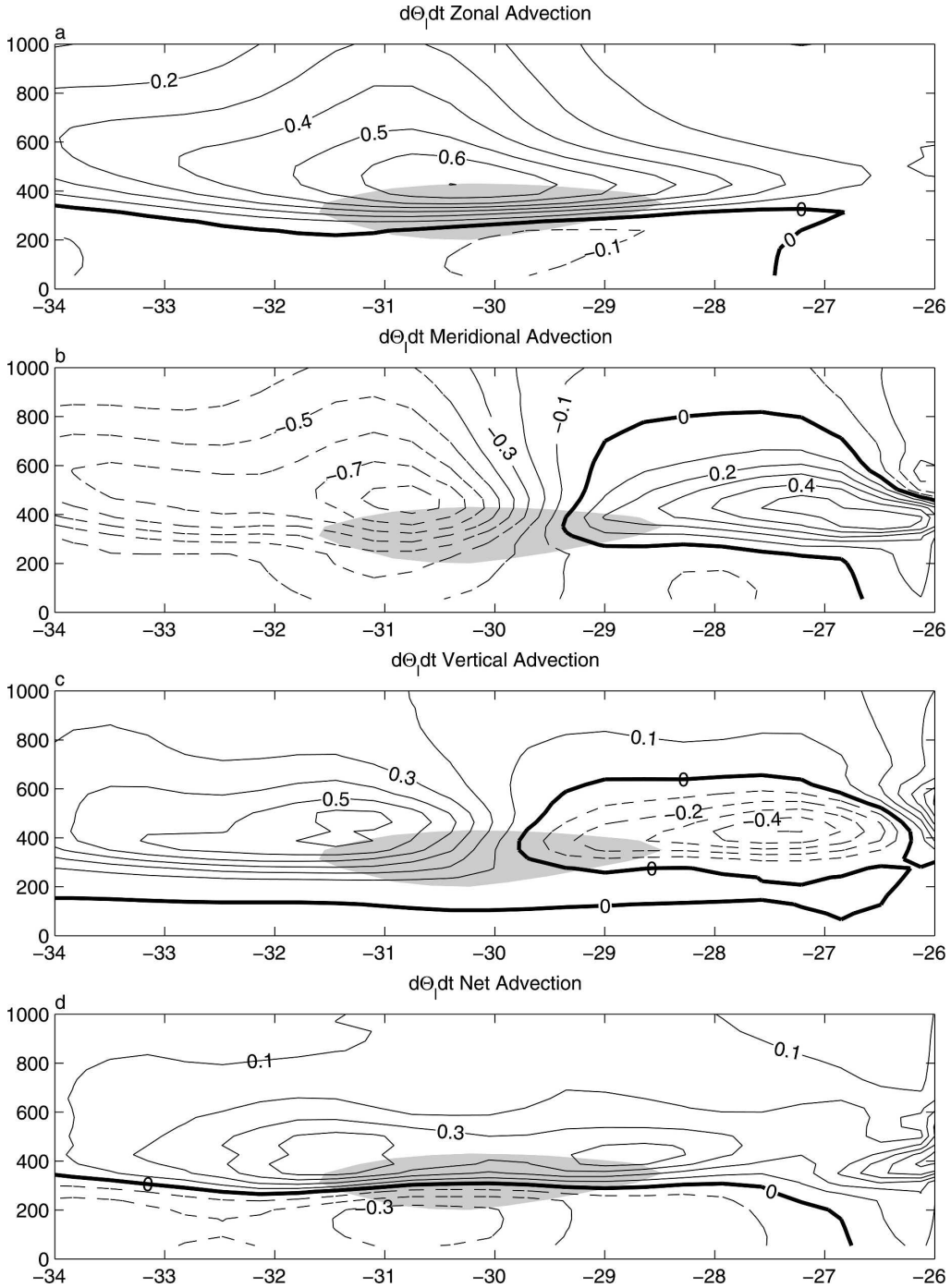

FIG. 11. Meridional cross section of advective terms in the liquid water potential temperature budget at 72.8°W, averaged for 9–11 Oct 2000. (a) Zonal advection, (b) meridional advection, (c) vertical advection, and (d) net advection. Contours in K h^{-1}. In all panels, vertical axis is height ASL (m) and horizontal axis is latitude (°). Shading marks regions with $V > 19$ m s^{-1}.

height level between 1000 and 850 hPa, indicative that the relevant variations of the geopotential (or pressure) gradient are "deep" rather than pure undulations of the MBL. Figure 13 shows that farther from the coast, and to the south, the relationship between V and the meridional PG diminishes, since in that region the simple geostrophic balance relating V and the *zonal* pressure gradient is the relevant dynamical constraint. We

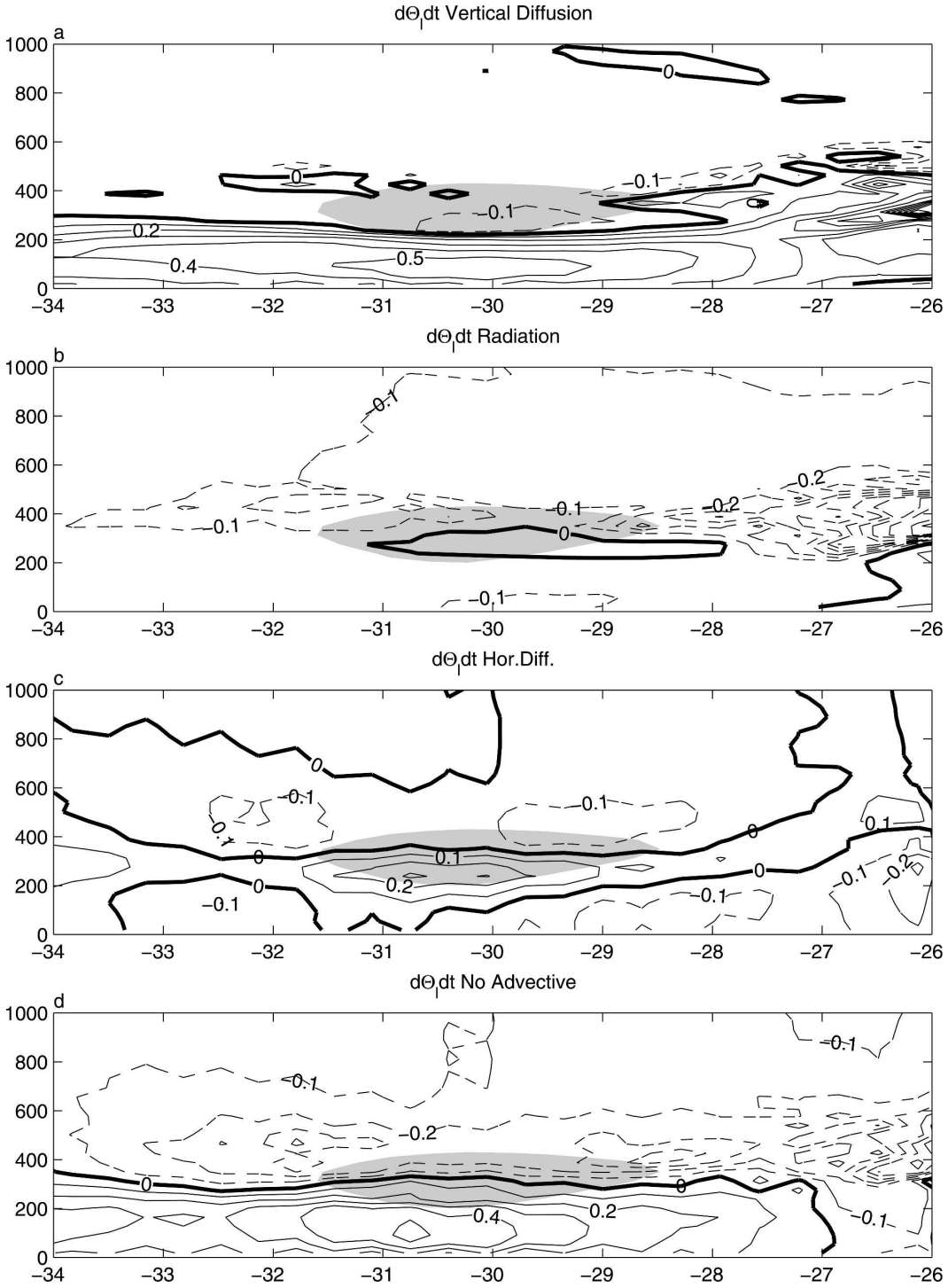

FIG. 12. Meridional cross section of nonadvective terms in the liquid water potential temperature budget at 72.8°W, averaged for 9–11 Oct 2000. (a) Turbulent vertical diffusion, (b) radiation, (c) horizontal diffusion, and (d) net nonadvective tendencies. Contours in K h^{-1}. In all panels vertical axis is height ASL (m) and horizontal axis is latitude (°). Shading marks region with $V > 19$ m s^{-1}.

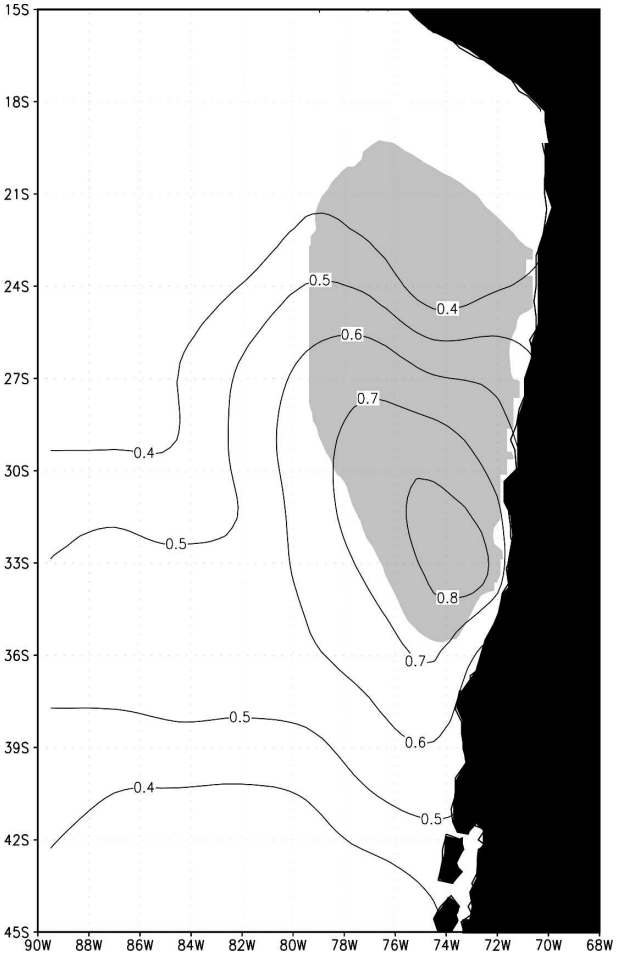

FIG. 13. Correlation coefficient squared (r^2) between collocated values of meridional surface wind speed (from QuikSCAT data) and meridional gradient of the 900-hPa geopotential height field (from the NCEP–NCAR reanalysis). Shading denotes area with mean meridional surface wind speed greater than 8 m s^{-1}. Period considered is Sep–Dec 2000–01.

speculate that in the jet region the high correlation between V and the meridional PG is associated with the blocking of the low-level zonal flow by the prominent coastal range along central Chile (average elevation of 1000 m ASL; see Fig. 1a).

c. Role of zonal flow (and diurnal cycle)

The magnitude of the zonal flow in (9) depends on the horizontal temperature gradients. Moreover, (9) and (10) indicate that $U/V \sim -(\partial\Theta_l/\partial y)/(\partial\Theta_l/\partial x)$. A larger difference between the mean ocean and land temperatures reduces the magnitude of U relative to V. On the other hand, the small diurnal cycle of this CJ (as shown in GM05) is explained by the fact that the relevant zonal wind in this conceptual model is not a sea breeze ($U>0$), but a synoptically induced easterly wind.

d. Role of turbulence (and MBL depth)

We have shown that the latitudinal position of the CJ is related to the balance between meridional pressure gradient acceleration and turbulent friction. We explore the sensitivity of the model results to the turbulent friction by performing a sensitivity analysis on the oceanic surface roughness. The model run used so far is considered a control run that computes the surface roughness (Z_o) over the sea with Charnock's formula relating Z_o to the friction velocity (U^*). For the present conditions, this method produces Z_o values between 0.0001 and 0.0010 m. A sensitivity run was then performed that used a constant roughness $Z_o = 0.1000$ m over all oceanic points.[1] In the sensitivity run the wind field also develops a coastal jet, but it is located to the south and nearer to the coast than the jet in the control run (positions of maximum low-level wind speed are marked by filled circles in the panels of Fig. 14). The magnitude of the jet is a few meters per second smaller than the original jet. One important difference between both runs is illustrated in Fig. 14, where contours of the mean MBL height have been drawn for both model runs. The sensitivity run develops a significantly deeper MBL, especially close to the coast, where the differences can be > 200 m. It must be noted that the sensitivity run has a smaller shear in the MBL, but it develops a deeper and more turbulent MBL. The reason appears to be in the stability capping the MBL. In the sensitivity run the zonal wind is weaker and the stability capping the MBL is smaller than in the control run, thus allowing the formation of a deeper MBL.

6. Concluding remarks

We have described the momentum and related balances that support the existence of a low-level jet along the western coast of South America. The picture emerging from these results relates the meridional jet to a condition in which the extratropical synoptic variability induces a PG force directed to the north along the coast of north-central Chile. As in the works that have addressed the CJ off the California coast, we find that here also the cross-shore flow plays a fundamental role in the dynamics of this CJ. The very steep coastal terrain in this region precludes the development of a significant easterly low-level wind that would geostrophically balance this pressure gradient. Instead, the meridional flow accelerates until turbulent friction in the MBL balances the meridional pressure gradient. At higher levels, the topographic inhibition of the easter-

[1] The control and sensitivity model runs described in this section were started at 0000 UTC 8 October 2000.

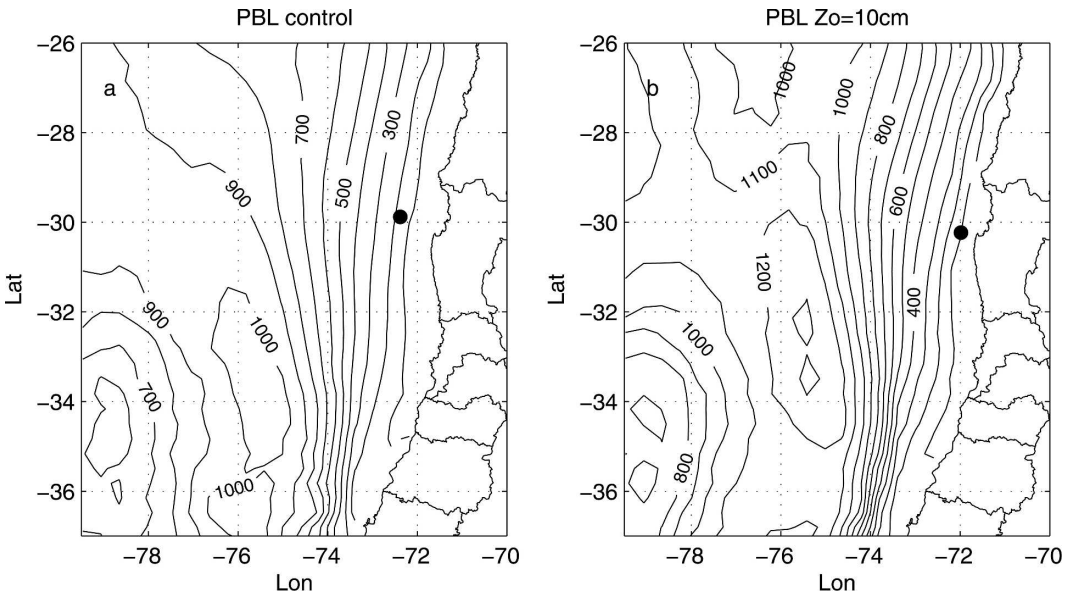

FIG. 14. Mean MBL heights computed by the model for the period 9–11 Oct 2000. (a) Control run and (b) run with Z_o = 0.10 m over ocean. Filled circles at ~30°S mark location of maximum mean wind speed below 3000 m ASL.

lies relaxes, and a small easterly flow ensues. In spite of its small magnitude, this easterly flow turns out to be very important in the temperature budget of the layer capping the MBL. Moreover, it partially controls the depth of the MBL by enhancing the stability of the capping layer above. Thus, our results suggest that the physical processes controlling the CJ in this region are similar to those discussed by Chao (1985) and found in the idealized simulations of Cui et al. (1998).

Model and observations suggest that the low-level winds have a significant diurnal cycle only close to the coast, where the surface winds diminish greatly during the night. This should result in the development of large horizontal mesoscale shear, which we speculate is the source of mesoscale vortices not infrequently observed in the stratocumulus layer off the coast. Quantitative analysis of the diurnal cycle of this CJ, though, has fallen beyond the scope of this work, and will be addressed in the future.

Acknowledgments. We are grateful to two anonymous reviewers who provided useful suggestions that improved the paper. This research was supported by FONDECYT (Chile) Grant 1020833.

REFERENCES

Bielli, S., P. Barbour, R. Samelson, E. Skyllingstad, and J. Wilczak, 2002: Numerical study of the diurnal cycle along the central Oregon coast during summertime northerly flow. *Mon. Wea. Rev.,* **130,** 992–1008.

Bridger, A. F. C., W. C. Brick, and P. F. Lester, 1993: The structure of the marine inversion layer off the central California coast: Mesoscale conditions. *Mon. Wea. Rev.,* **121,** 335–351.

Brost, R. A., J. C. Wyngaard, and D. H. Lenshow, 1982: Marine stratocumulus layers. Part II: Turbulence budgets. *J. Atmos. Sci.,* **39,** 818–836.

Burk, S. D., and W. T. Thompson, 1996: The summertime low-level jet and marine boundary layer structure along the California coast. *Mon. Wea. Rev.,* **124,** 668–686.

Chao, S., 1985: Coastal jets in the lower atmosphere. *J. Phys. Oceanogr.,* **15,** 361–371.

Cui, Z., M. Tjernstrom, and B. Grisogono, 1998: Idealized simulations of atmospheric coastal flow along the central coast of California. *J. Appl. Meteor.,* **37,** 1332–1363.

Deardorff, J. W., 1976: Usefulness of liquid-water potential temperature in a shallow-cloud model. *J. Appl. Meteor.,* **15,** 98–102.

Garreaud, R. D., and R. C. Muñoz, 2005: The low-level jet off the west coast of subtropical South America: Structure and variability. *Mon. Wea. Rev*., **133,** 2246–2261.

——, J. Rutllant, and H. Fuenzalida, 2002: Coastal lows in north-central Chile: Mean structure and evolution. *Mon. Wea. Rev.,* **130,** 75–88.

Gayno, G. A., 1994: Development of a high-order, fog-producing boundary layer model suitable for use in numerical weather predicition. M.S. thesis, Dept. of Meteorology, The Pennsylvania State University, 104 pp.

Grell, G. A., J. Dudhia, and D. R. Stauffer, 1994: A description of the fifth-generation Penn State University/NCAR Mesoscale Model (MM5). NCAR Tech. Note NCAR/TN-398+STR, 122 pp.

Lester, P. F., 1985: Studies of the marine inversion over the San Francisco Bay Area: A summary of the work of Albert Miller 1961–1978. *Bull. Amer. Meteor. Soc.,* **66,** 1396–1402.

Parish, T., 2000: Forcing of the summertime low-level jet along the California coast. *J. Appl. Meteor.,* **39,** 2421–2433.

Pomeroy, K. R., and T. Parish, 2001: A case study of the interaction of the summertime coastal jet with the California topography. *Mon. Wea. Rev.,* **129,** 530–539.

Shafran, P. C., N. L. Seaman, and G. A. Gayno, 2000: Evaluation of numerical predictions of boundary layer structure during the Lake Michigan Ozone Study (LMOS). *J. Appl. Meteor.,* **39,** 412–426.